JOURNAL OF SOLID STATE CHEMISTRY 90, 331–343 (1991)

Crystal Structure and Mössbauer Spectroscopy of $Y_2SrFeCuO_{6.5}$, a Double Layer Perovskite Intergrowth Phase

J. S. KIM, J. Y. LEE, J. S. SWINNEA, AND H. STEINFINK[1]

Materials Science and Engineering, Department of Chemical Engineering, The University of Texas at Austin, Austin, Texas 78712

W. M. REIFF

Department of Chemistry, Northeastern University, Boston, Massachusetts 02115

AND P. LIGHTFOOT, S. PEI, AND J. D. JORGENSEN

Argonne National Laboratory, Argonne, Illinois 60439

Received June 26, 1990

The crystal structure of $Y_2SrFeCuO_{6.5}$ was determined from single-crystal X-ray and neutron powder diffraction studies. M_r = 488.81, orthorhombic, *Ibam*, a = 5.4036(8)[5.4149(1)] Å, b = 10.702(1)[10.7244(1)] Å, c = 20.250(2)[20.2799(2)] Å; values in square brackets are neutron data. V = 1171.0(4), Z = 8, D_x = 5.544 g cm^{-3}, λ = 0.71069 Å, μ = 345.1 cm^{-1}, R = 0.048 for 567 observed reflections. The Fe/Cu atoms occupy randomly the approximate center of oxygen pyramids. The pyramids share the apical oxygen and articulate laterally by corner sharing of oxygen to form a double pyramidal layer perpendicular to c. The pyramidal slabs are separated by double layers of Y that are in 7-fold coordination to oxygen, forming a defect fluorite unit. Mössbauer spectra indicate a unique iron environment and magnetic ordering at about 265 K. The paramagnetic phase coexists with the magnetic phase over an approximate temperature range 300–263 K, characteristic of magnetic ordering in 2-D magnetic structures. The isomer shift, 0.26, and quadrupole splitting, 0.56 mm sec^{-1}, are consistent with Fe^{3+} in 5-fold coordination and H_{int} values also indicate classic high spin Fe^{3+}. The average Y–O bond length is 2.331(6) Å and Sr is in a dodecahedral environment in which, however, two oxygen atoms at the corners of the cube are missing. The average Sr–O bond length is 2.793(10) Å. The structure is derived from the Ruddlesden–Popper phase $Sr_{n+1}Ti_nO_{3n+1}$ with n = 2.

Introduction

Intergrowth crystal structures in inorganic systems have provided a fertile field of solid state chemical research for many years and the discovery of high-T_c superconducting cuprates has focused attention on intergrowth structures based on perovskite blocks. Aurivillius (*1–3*) described the preparation and crystal structures of a series of compounds in which layers formed by two or more sequences of perovskite units are separated by Bi_2O_2 layers. The octahedral interstices of the perovskite units are occu-

[1] To whom correspondence should be addressed.

0022-4596/91 $3.00

pied by transition metals such as Ti, Nb, and Ta, and the dodecahedral interstices by alkaline earth ions. Ruddlesden and Popper (R-P hereafter) (*4*) have described intergrowth structures with the general formula $Sr_{n+1}Ti_nO_{3n+1}$ where n is the number of perovskite layers. Indeed, La_2CuO_4 corresponds to the $n = 1$ phase in which the decreased ionic charge of the octahedral ion is compensated by the increased ionic charge of the dodecahedral ion. The attempt to replace La by Y in the superconductor $La_{2-x}M_xCuO_4$ (M = Sr, Ba) (*5*) gives rise to a new structure in which the apical bridging oxygen of the double octahedral sheet is removed at the Y level to leave Cu in square pyramidal coordination. This radical change in crystal structure produces the well known high-T_c superconductor $YBa_2Cu_3O_7$, 123. Extensive isomorphous replacement studies have shown that the presence of Y and/or Ca in these structures invariably removes an apical oxygen from the octahedron around the copper ion to form at first a square pyramid and eventually a square planar coordination when Ca flanks both sides of the CuO_2 layer.

Single phase $YSr_2Cu_3O_7$ can not be prepared but the substitution of other metals for Cu, e.g. Fe, Co, Al, Pb, stabilizes the Sr 123 structure to the point where all of the Ba can be replaced by Sr (*6*). The superconducting transition temperature is adversely affected by these substitutions and eventually the material becomes semiconducting. Sunshine *et al.* (*6*) investigated the crystal structures of $YSr_2Cu_{2.33}Al_{0.67}O_{6.63}$ and $YSr_2Cu_{2.52}Pb_{0.48}O_6$ using single crystal X-ray diffraction procedures and we attempted to grow Fe-containing single crystals using Bi_2O_3 as a flux and mineralizer. X-ray powder diffraction patterns from mixtures of Y_2O_3, $SrCO_3$, CuO, and Fe_2O_3 in various proportions indicated a new phase in addition to a 123 phase (presumably $YSr_2Cu_{3-x}Fe_xO_7$). A mixture in which the stoichiometry was nearly $Y_2SrCuFe$ yielded a product that was judged to be almost a single phase of the unknown compound on the basis of its X-ray powder diffraction pattern. Repeated experiments near this composition produced single crystals of this new phase in the contact zone with the alumina crucible. We report here the crystal structure of this new cuprate phase.

Experimental

Sample Preparation

Samples with composition $Y_1Sr_2Cu_{3-x}M_xO_{7-\delta}$ (M = Co and Fe) were prepared by solid state reactions between $SrCO_3$, Y_2O_3, CuO, and Fe_2O_3 (or Co_3O_4). Powders were mixed and heated in air at temperatures between 1000 and 1100°C for 10–20 hr. Single crystal growth experiments of $YSr_2Cu_{3-x}M_xO_{7-\delta}$ (M = Co and Fe) were not successful at the stoichiometric compositions. With excess copper, $Sr_{14}Cu_{24}O_{48}$-type single crystals were obtained at a crystal growth reaction temperature of 1040°C. With PbO as a flux, single crystals with $a \cong b \cong c \approx 3.84$ Å were obtained from the nominal composition $YSr_2Cu_{3-x}M_xPb_{0.5}O_y$. With Bi_2O_3 as a flux, the nominal compositions $YSr_2Cu_2FeBi_xO_y$ with $x = 0.1$–0.5 were fired over a temperature range 1020–1110°C. Platy single crystals were found at the contact zone between the sample and the alumina boat. The optimum condition for growing these single crystals was $x = 0.3$–0.4 at a temperature of 1100°C. A single crystal was selected and analyzed by standardless energy dispersive X-ray spectroscopy, EDX. Its composition was approximately 40Y : 25Sr : 20 Cu : 15Fe; no Al was detected. Oscillation, Weissenberg, and precession photographs showed that the crystal was orthorhombic with cell dimensions $a = 5.43$ Å, $b = 10.67$ Å, and $c = 20.2$ Å, space group *Ibam*. Based on the stoichiometry determined eventually from the single crystal structure analysis, synthesis reactions using mixtures in the stoichiometric ratio produced a single

TABLE I

SUMMARY OF DATA COLLECTION AND STRUCTURE REFINEMENT FOR $Y_2SrCuFeO_{6.5}$

Formula weight	488.81
Crystal system	Orthorhombic
a(Å)	5.4036(8)
b(Å)	10.702(1)
c(Å)	20.250(2)
V (Å^3)	1171.0(4)
Space group	*Ibam*
Z	8
D_x(g cm^{-3})	5.544
μ(cm^{-1})	345.1
λ(Å)	0.71069
F(000)	1784
Dimensions (μm)	120 × 100 × 20
Mode	$\theta - 2\theta$
Max. 2θ	60
Scan rate (deg min^{-1})	variable, $\sigma(I)/I$ = 0.02
Scan width	2 + 0.70 tan θ
hkl min	−7, −14, 0
hkl max	7, 14, 28
Reflections, measured	3250
Reflections, unique	882
R_{int}	0.046
$\geq 5\ \sigma$(F)	567
Transmission factor	0.5441–0.0959
Standard reflections	165, $1\bar{6}5$, $\bar{3}25$, $3\bar{2}5$
Number of variables	41
w^{-1}	$\sigma^2(F_0) + 0.0004F_0^2$
Goodness of fit, S	1.38
Function minimized	$\Sigma w(\|F_0 - F_c\|)^2$
R, wR	0.048, 0.042
max shift/e.s.d.	0.002
$\Delta\rho$, max, min (e Å^{-3})	+2.1, −2.3
g, extinction	2.3(3) × 10^{-8}

phase, ceramic material when reacted in air at 1030°C for 12 hr with subsequent regrinding and refiring at 1030°C.

X-Ray Structure Determination

A single crystal that was first examined by Weissenberg and precession photography was transferred to a Krisel automated Picker diffractometer equipped with an incident beam monochromator, $\lambda(MoK_\alpha)$ = 0.71069 Å. The conditions for the data collection, data reduction, and refinement are shown in Table I. The lattice constants were obtained from a least-squares calculation of precisely determined 2θ values of 38 reflections between 25 and 27 degrees. The variations in the intensities of the four standard reflections measured after every 180 min fluctuated randomly ±2%. Estimated standard deviations, $\sigma(F_0)$, were obtained from counting statistics. Absorption corrections were calculated using ORABS (*7*); direct methods calculations and least-squares refinements were carried out with SHELX 76 (*8*). The atomic scattering factors for neutral atoms and corrections for anomalous dispersion were obtained from the *International Tables* (*9*). An extinction correction, g, was applied using the expression $F = F(1 - gF^2/\sin\theta)$.

The lattice constants are related to that of perovskite, a_p = 3.8 Å, by $\sqrt{2}\ a_p$, $2\sqrt{2}\ a_p$ and the c-axis value is similar to those of $Sr_3Ti_2O_7$ (*4*), $Tb_2SrFe_2O_7$ (*10*), $La_2BaFe_2O_7$ (*10*), and $La_{2-x}A_{1+x}Cu_2O_6$ (*11*). The rare earth-containing compounds are based on the structure of the parent compound $Sr_3Ti_2O_7$, which is a member of the series $Sr_{n+1}Ti_nO_{3n+1}$, and are designated as Ruddleston–Popper phases (*4*). A direct methods and Patterson calculations yielded the cation positions that indicated that the structure was related to the $Sr_3Ti_2O_7$ parent. Difference electron density maps revealed all oxygen atoms. The final positional parameters, thermal displacement parameters, and a variable occupancy factor for Fe are listed in Table II. A Table of F_0, F_c and $\sigma(F_0)$ has been deposited.[1] Table III lists the X-ray powder diffraction pattern obtained with

[1] See NAPS document No. 04811 for 7 pages of supplementary material. Order from ASIS/NAPS, Microfiche Publications, P.O. Box 3513, Grand Central Station, NY 10163. Remit in advance $4.00 for microfiche copy or for photocopy $7.75 up to 20 pages plus $.30 for each additional page. However, there is a billing and handling charge for this service of $15. Foreign orders add $4.50 for postage and handling, for the first 20 pages, and $1.00 for additional 10 pages of materials, $1.50 for postage of any microfiche orders.

TABLE II

POSITIONAL AND THERMAL DISPLACEMENT PARAMETERS FOR $Y_2SrCuFeO_{6.5}$. THE FIRST LINE OF DATA FOR EACH ATOM IS FROM THE X-RAY AND THE SECOND LINE FROM THE NEUTRON REFINEMENT[a]

Atom	x	y	z	U_{11}	U_{22}	U_{33}	U_{23}	U_{13}	U_{12}	B(Å^2)
Sr	0.2061(3)	0.3658(1)	0	0.0126(6)	0.0108(7)	0.0190(8)	0	0	0.0001(7)	1.12(3)
	0.2068(6)	0.3656(4)	0							1.20(5)
Fe[b]	0.7173(3)	0.3833(1)	0.0985(1)	0.0047(6)	0.0050(7)	0.0146(9)	0.0003(6)	−0.0007(6)	−0.0003(5)	0.64(3)
	0.7162(3)	0.3833(2)	0.09808(6)							0.31(2)
Y	0.2097(2)	0.3620(1)	0.1843(1)	0.0059(4)	0.0052(4)	0.0055(5)	−0.0001(4)	−0.0000(4)	−0.0001(4)	0.44(2)
	0.2083(3)	0.3622(2)	0.18389(7)							0.24(2)
O1	0.1942(20)	0.1108(9)	0	0.0111(22)						0.88(17)
	0.1944(7)	0.1094(3)	0							0.64(5)
O2	0	½	0.1062(6)	0.0075(20)						0.59(16)
	0	½	0.1062(2)							0.65(6)
O3	0	½	¼	0.0088(31)						0.69(24)
	0	½	¼							0.31(9)
O4	½	0.2779(8)	¼	0.0038(21)						0.30(17)
	½	0.2784(3)	¼							0.55(6)
O5	0.4559(15)	0.2532(7)	0.1088(4)	0.0084(14)						0.66(11)
	0.4552(5)	0.2534(2)	0.1083(1)							0.44(4)
O6	0	0	0.3565(6)	0.0058(20)						0.46(16)
	0	0	0.3554(2)							0.22(5)

[a] The form of the anisotropic displacement parameter for the X-ray refinement is $\exp[-2\pi^2(U_{11}a^{*2}h^2 + \cdots + 2U_{23}b^*c^*kl + \cdots)]$ and $B_{eq} = 8\pi^2U_{eq}$, where U_{eq} is calculated from ⅓ of the trace of the diagonalized tensor. The neutron diffraction values are from an isotropic refinement.

[b] The site occupancy from the X-ray data refinement is 1.045(7) corresponding to Fe : Cu = 1.2 : 0.8. The neutron data refinement is based on Fe : Cu = 1 : 1.

Cu$K\alpha$ and a diffractometer equipped with a diffracted beam monochromator.

Mössbauer Spectroscopy

Mössbauer spectra were obtained on a conventional constant acceleration spectrometer operated in conjunction with a Canberra Series 35 multichannel analyzer, by using a 100-mCi ^{57}Co in rhodium metal matrix γ-ray source. Temperature control was achieved by using an uncalibrated silicon diode coupled to a Lake Shore Cryotronics Model DT-500 C set point controller. Temperature measurements were made with a digital voltmeter by using a calibrated silicon diode driven by a 10-μA constant current source. Spectra below room temperature were obtained by using either a flow-type or an exchange-type Janis cryostat in either a horizontal or a vertical mode. Isomer shifts are relative to metallic Fe at room temperature.

Neutron Powder Diffraction Structure Determination

Neutron powder diffraction data were collected at 295 and 10 K on the Special Environment Powder Diffractometer (SEPD) at the Intense Pulsed Neutron Source, Argonne (*12*). Lattice constants at 295 K are a = 5.4149(1), b = 10.7244(1), c = 20.2799(2) Å; they differ significantly from the X-ray values. For the low temperature data collection, the sample was contained in an indium-sealed vanadium can with 1 atm (at room-temperature) of helium exchange gas. In order to investigate the room temperature nuclear structure, data from the high-resolution ($\Delta d/d$ = 0.0034) backscattering detector banks (2θ = 150°) were used. In order to study the magnetic structure, it is crucial to obtain higher d-spacing data; thus, data from the 2θ = 60° ($\Delta d/d$ = 0.0080) detectors were used.

Initial Rietveld refinement (*13*) of the room temperature data was carried out assuming the model obtained from the single crystal X-ray study. Convergence was soon achieved, giving a very good fit to the data (R_{wp} = 5.85%, R_{exp} = 3.25%), for a total of 2200 reflections in the range $0.52 < d < 3.20$ Å. Careful scrutiny of the final observed and calculated diffraction profiles. Fig. 1, revealed no extraneous peaks, suggesting

TABLE III

OBSERVED AND CALCULATED *d*-SPACINGS AND INTENSITIES FOR $Y_2SrCuFeO_{6.5}$ BASED ON THE PARAMETERS FROM TABLE II

h	*k*	*l*	d_{obs}	d_{calc}	$I_{Rel, obs}$	$I_{Rel, calc}$
0	2	0	5.348	5.351	<1	1.2
0	0	4	5.050	5.063	3.3	2.1
1	1	0	4.818	4.824	1.9	1.4
1	2	1	3.732	3.737	3.9	3.3
1	1	4	3.490	3.492	1.9	1.5
0	0	6	3.371	3.375	4.3	3.7
1	2	3	3.310	3.313	7.6	6.1
0	2	6	2.857	2.854	1.2	0.1
1	2	5	2.772	2.772	100	100
2	0	0	2.703	2.702	14.8	14.6
0	4	0	2.675	2.675	16.9	17.9
2	1	1	2.598	2.598	4.8	4.7
1	4	1	2.382	2.381	3.2	2.6
1	2	7	2.304	2.302	1.8	2.3
1	3	6	2.234	2.233	3.9	4.5
2	1	5	2.200	2.200	2.8	3.2
2	3	1	2.143	2.142	3.3	3.9
2	0	6	2.109	2.109	5.2	5.1
0	4	6	2.100	2.097	6.2	6.1
0	0	10	2.025	2.025	6.3	8.8
1	2	9	1.964	1.936	1.2	3.9
2	4	0	1.903	1.901	14.5	23.9
2	0	8	1.848	1.847	1.1	1.5
0	4	8	1.841	1.839	1.3	1.5
0	0	12	1.685	1.687	1.4	1.8
2	5	1	1.674	1.672	2.0	2.0
1	2	11	1.658	1.657	3.5	3.7
2	4	6	1.658	1.656		1.2
2	0	10	1.621	1.620	4.4	6.1
3	2	5	1.574	1.573	7.5	9.7
1	6	5	1.564	1.563	9.7	13.6

the absence of any superstructure or lowering of symmetry from that determined by the X-ray study. In addition, all structural parameters are in good agreement with those obtained by X-rays, and all the temperature factors refine to chemically sensible values, Table II.

In order to analyze the 10 K data, accurate structural parameters were first obtained by analysis of backscattering data in the range $0.5 < d < 2.0$ Å. Any magnetic contribution to the refinement was thus minimized. The structural parameters were then fixed, and various magnetic models tested using the high *d*-spacing data ($1.0 < d < 5.5$) from the low-angle detector bank. Several new peaks were observed, all of which could be indexed on the basis of a *primitive* cell of the same size as the original body-centered nuclear cell.

Elemental Analysis, Thermogravimetric Analysis, and Magnetic Susceptibility

Elemental analysis on powders and single crystals were obtained by EDX using a JEOL JSM-35C scanning electron microscope equipped with a Kevex spectrometer. Thermogravimetric analysis was carried out with a Perkin–Elmer TGA-7 system. Magnetic susceptibility data were determined from 2.2 to 350 K using a computer-automated Faraday balance using fields of 5.2, 15.8, and 19.5 kG.

Results and Discussion

Crystal Structure

The crystal structure of $Y_2SrCuFeO_{6.5}$ is illustrated in Fig. 2. The structure consists of sheets of apex-sharing oxygen pyramids whose approximate centers are randomly occupied by Fe and Cu. They articulate by corner sharing of the equatorial oxygen ions into two-dimensional slabs that are separated by a double layer of Y^{3+}. The Y^{3+} ions are in 7-fold coordination; the seven oxygen ions are located at the corners of a cube with the eighth corner vacant. The yttrium–oxygen configuration can be considered a defect fluorite unit and those units articulate by edge sharing within a given Y level and by edge sharing to the adjacent Y level. The oxygen atoms O3 and O4 constitute the layer separating the Y sheets and contain the vacant site at $\frac{1}{2}, \frac{1}{2}, \frac{1}{4}$. The Y environment is intermediate between that of the fluorite structure and that of the C–Y_2O_3 structure. The oxygen ions, O4, are displaced 0.30 Å from the idealized $\frac{1}{2}\ \frac{1}{4}\ \frac{1}{4}$ and $\frac{1}{2}\ \frac{3}{4}\ \frac{1}{4}$ positions toward the vacant site. The base of the pyra-

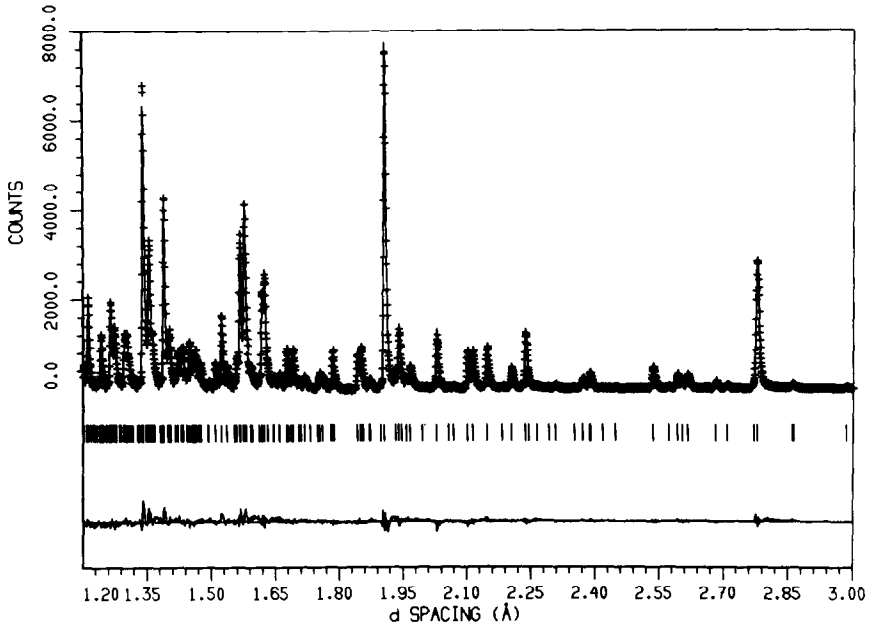

FIG. 1. Portion of the Rietveld refinement profile for $Y_2SrFeCuO_{6.5}$, *Ibam*, at 295 K. Plus marks (+) are the raw data, solid line is the calculated profile. Tick marks below the profile mark the positions of allowed reflections. A difference curve (observed-calculated) is plotted beneath.

mid is formed by O2, O5, and O6. Two of these, O2 and O5, lie in a plane while O6 is displaced from it 0.7 Å toward the vacant site; (Fe, Cu) is 0.2 Å above the plane. The Sr ion is at the level of the apical oxygen, O1 and is in 10-fold coordination. This interstice corresponds to the dodecahedral site in perovskite, but in this structure one edge of the oxygen cube is missing.

The sequence of layers can be described as a double pyramidal layer $[(Cu_1Fe_1)O_5]^{5-}$ flanked by defect fluorite blocks of $(Y_2O_{1.5})^{3+}$ and Sr^{2+} as the counter ion. An equivalent description is obtained by using the layer sequence $SrO–[(Cu_{0.5}Fe_{0.5})O_2]^{1.5-}–(Y_2O_{1.5})^{3+}–[(Cu_{0.5}Fe_{0.5})O_2]^{1.5-}–SrO$.

The occupancy factor of the Fe/Cu site was refined in the X-ray structure analysis in order to obtain information about the Fe : Cu ratio. The X-ray scattering factors of these two ions are so similar that their identification in a specific crystallographic site usually must depend on differences in coordination geometry. Attempts to order Fe and Cu in the structure by lowering the space group symmetry to *Iba*2 were fruitless. Least-squares refinements converged to *R* values between 5 and 5.5% with unrealistic bond lengths and temperature factors. Since the cations appeared to be randomly distributed over this position syntheses of this compound were carried out in which Fe : Cu ratios were varied. Indeed, the products from a synthesis in which Cu : Fe = 1.2 : 0.8 showed a second phase whose diffraction lines are consistent with the 123 structure type and is probably due to $YSr_2Cu_{3-x}Fe_xO_y$. TGA experiments using such samples showed the typical sorption–desorption curves of O_2 for 123 structures. When the Fe concentration was increased, e.g., 1.2Fe : 0.8 Cu, the product contained $YFeO_3$. On the basis of the syntheses results it is concluded that the Fe : Cu ratio is 1 : 1

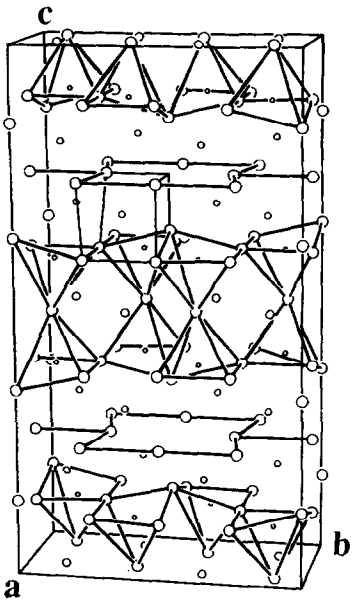

FIG. 2. The crystal structure of $Y_2SrFeCuO_{6.5}$. Large circles are oxygen atoms, intermediate circles are Y, and small circles are Fe/Cu. Heavy lines connect oxygen atoms; the thin lines outline the coordination polyhedron around one Y.

within the detectability limits of the X-ray powder diffraction technique. The neutron diffraction results similarly led to the conclusion that there is no crystallographic ordering of the Fe and Cu atoms and refinement converged to a good fit with the experimental data for a stoichiometric composition Fe : Cu = 1 : 1. This contrasts with the results for the structure of $YBaCuFeO_5$ (*14*) in which apex-sharing double layers of pyramids are present. The structural refinement in *P*4 *mm* of powder neutron diffraction data allows two crystallographically distinct positions for the Cu–Fe sites and yields two distributions, $(Fe_{0.62}Cu_{0.38})$ and $(Fe_{0.38}\ Cu_{0.62})$. The Fe-rich site shows a distinct lengthening of the apical *M*–O bond length while in the Cu-rich site the square pyramid has equal *M*–O bond lengths.

The bond distances and angles in this structure from both the X-ray and the neutron data refinements are shown in Table IV. The X-ray values are based on the lattice parameters shown in Table I while the neutron values are based on the slightly different lattice parameters (vide supra). The average bond length Sr–O is 2.793(10) Å and Y–O is 2.331(6) Å (x-ray values) and these are within the normal range observed in other structures. The Fe/Cu–O distances correspond most closely to those reported

TABLE IV

SELECTED BOND DISTANCES (Å) AND ANGLES (deg) FOR $Y_2SrFeCuO_{6.5}$

	X-ray	Neutron
Sr–O1	2.730(1)	2.748(5)
Sr–O1	2.677(1)	2.669(5)
Sr–O1	2.777(11)	2.787(5)
Sr–O1	2.649(11)	2.654(5)
Sr–2O2	2.815(9)	2.823(4)
Sr–2O5	2.852(8)	2.844(3)
Sr–2O5	2.882(8)	2.884(3)
Y–O2	2.443(8)	2.436(3)
Y–O3	2.289(1)	2.292(2)
Y–O4	2.245(4)	2.259(2)
Y–O4	2.302(6)	2.311(3)
Y–O5	2.336(8)	2.344(3)
Y–O5	2.395(8)	2.400(3)
Y–O6	2.307(4)	2.305(2)
Fe/Cu–O1	2.002(2)	1.994(1)
Fe/Cu–O2	1.979(2)	1.989(1)
Fe/Cu–O5	1.994(8)	1.995(3)
Fe/Cu–O5	1.960(8)	1.996(3)
Fe/Cu–O6	1.940(6)	1.956(2)
O5–O6	2.743(8)	
O6–O2	2.805(4)	
O2–O5	2.721(7)	
O5–O5	2.7027(5)	
O1–Fe/Cu–O2	96.1(5)	96.0(2)
O1–Fe/Cu–O5	94.7(4)	95.1(1)
O1–Fe/Cu–O5	99.8(4)	100.0(1)
O1–Fe/Cu–O6	114.2(4)	114.9(2)
O2–Fe/Cu–O5	168.3(4)	168.0(2)
O2–Fe/Cu–O5	87.4(2)	87.2(1)
O2–Fe/Cu–O6	91.4(2)	91.13(9)
O5–Fe/Cu–O5	86.23(7)	86.25(7)
O5–Fe/Cu–O6	88.4(2)	88.42(9)
O5–Fe/Cu–O6	145.9(4)	145.1(1)
Fe/Cu–O1–Fe/Cu	172.0(6)	

for $Cu_{0.62}Fe_{0.38}$–O in $YBaCuFeO_5$ (*14*). It is noteworthy that the shortest bond length, Fe/Cu–O6, occurs for the oxygen ion that is displaced 0.7 Å from the basal plane of the pyramid toward the vacant site.

A bond valence sum calculation (*15*) for the Fe/Cu–O coordination using the expression $S = \Sigma \exp[(r_0 - r_i)/B)]$, where $B = 0.37$, and $r_0 = 1.719$, the average value for $r_0(Fe^{3+}–O^{2-})$ and $r_0(Cu^{2+}–O^{2-})$ and $r_0(Cu^{2+}–O^{2-})$, yields $S_{Fe/Cu} = 2.52$, reinforcing the conclusion that the site is randomly occupied by equal amounts of Fe^{3+} and Cu^{2+}.

Thermogravimetric analysis (TGA) of a sample heated and cooled in air between room temperature and 900°C showed no weight loss or gain. The placement of even a partial oxygen atom in the vacant site, 0 0 ¼, 4*b* of space group *Ibam*, results in its removal during least-squares refinement. This phase does not display a detectable oxygen variability. Syntheses were carried out in which Y was replaced by La, Ce, Pr, Nd, Gd, Er, and Lu. Only Gd and Er form this phase. As mentioned previously deviations from a 1 : 1 Fe/Cu ratio, if present at all, are very small. The mixture of oxides $Y_{1.75}Ca_{0.25}SrCuFeO_{6.5}$ yields a single phase but when Ca exceeds 0.25 other phases begin to appear in the X-ray diffraction diagram. Attempts to place Sr into the Y site did not yield single-phase products.

Neutron Diffraction

In order to analyze the 10 K neutron diffraction data, accurate structural parameters were first obtained by analysis of backscattering data in the range $0.5 < d < 2.0$ Å. Any magnetic contribution to the refinement was thus minimized. The structural parameters were then fixed, and various magnetic models were tested using the high-*d* spacing data ($1.0 < d < 5.5$) from the low-angle detector bank. Several new peaks were observed, confirming some type of 3-D antiferromagnetic ground state, consistent with the magnetic susceptibility data (vide infra). A 3-D ferromagnetic ground state would normally be expected to result only in the enhancement of the room temperature structural reflections since there is only one magnetic lattice for a simple ferromagnet. All of the additional peaks could be indexed on the basis of a *primitive* cell of the same size as the original body-centered nuclear cell.

In proposing magnetic models to fit these data, it is reasonable to assume that nearest neighbor interactions will be antiferromagnetic along 180° *M*–O–*M* superexchange pathways ($M = Fe^{3+}$, Cu^{2+}) (*16*). Such an ordering scheme is observed, for example, in the oxygen-deficient perovskite $Sr_2LaFe_3O_8$ (*17*), and in the layered cuprate La_2CuO_4 (*18*). The initial models therefore adopted this criterion. In addition, the moments were constrained to lie along a principal crystallographic axis, *a*, *b*, or *c*. These models failed to account for the observed scattering. Several models were then tested with ferromagnetic intralayer interactions and antiferromagnetic interlayer interactions, with the constraint that the resultant magnetic structure should be primitive rather than I-centered. None of these models adequately accounted for the observed scattering. Several problems with the nature of the data make an unambiguous magnetic structure determination very difficult: (i) inability to access the crucial high *d*-spacing reflections ($d > 6$ Å), hence inability to determine whether any superlattice is actually present, (ii) inability to distinguish between nuclear and magnetic scattering—the structure may undergo a subtle structural distortion at low temperature—(iii) low resolution for the $2\theta = 60°$ data, making unambiguous indexing of the magnetic peaks difficult. For these reasons, further studies of the magnetic structure of this phase were not pursued. It is interesting to note, however, that

to our knowledge, no magnetic structural studies for these type of phases ($Sr_3Ti_2O_7$-related structures) have been reported. These structures ($AO \cdot 2ABO_3$) may be regarded as intermediate between the 3-D perovskite (ABO_3) and 2-D K_2NiF_4 ($AO \cdot ABO_3$) structure types, and would therefore be of interest in studying pseudo-2D magnetic properties.

Mössbauer Spectroscopy

Mössbauer studies reveal that magnetic ordering begins below 300 K and the quadrupole split lines disappear completely at about 263 K. The spectra shown in Fig. 3 illustrate the transition from the rapidly relaxing paramagnetic to the 3-D magnetically ordered phase and saturation behavior. Table V lists the isomer shifts and internal magnetic field values. The extrapolation of H_{int} to zero field, Fig. 4, locates the Neél transition temperature at about 265 K.

In Table V are listed isomer shift values that are about 0.1 mm/sec smaller than those observed for FeO_6 chromophores and the quadrupole splitting is small and essentially temperature independent, consistent with Fe^{3+} in 5-fold coordination. H_{int} values are also fully consistent with high-spin Fe^{3+} (*19*). The spectra don't show any indications for two crystallographically different Fe^{3+} sites in contrast to the spectrum for YBaCu FeO_5 (*14*). In Fig. 3 the change in the spectra in the region between 300 and 77 K occurs as a result of the change in ratio of the strength of the electric quadrupole interaction, which is essentially temperature independent, and the magnetic hyperfine field, which decreases rapidly as the temperature approaches the Neél temperature near 265 K. The paramagnetic phase for which the atomic relaxation time is short compared to the nuclear precession frequency (*19*) persists down to 262.8 K. The persistence of the paramagnetic phase is a characteristic of a two-dimensional magnetic layer compound. At 77 K a Mössbauer spectrum typical for a magnetically ordered phase is observed although full saturation magnetization has not yet been achieved.

The analysis of the combined quadrupole interaction–Zeeman spectrum at 4.8 K permits the description of a possible 3-D-ordered magnetic state for $Y_2SrFeCuO_{6.5}$. On the assumption that the principal component of the electric field gradient tensor, V_{zz}, is positive and along the direction of the apical Fe–O bond, approximately parallel to the c-axis, the calculated angle θ between V_{zz} and the easy axis of magnetization is about 49° or close to 45° to the a–b plane.

Magnetic Susceptibility

For a system of noninteracting magnetic dipoles the total magnetic moment $\mu_T = [\Sigma_i \mu_i^2]^{1/2}$. Assuming spin-only combinations $\mu(Cu^{2+}) = \sqrt{3}$ and for high-spin Fe^{3+} $\mu = \sqrt{35}$ so that $\mu_T = \sqrt{38}$ or 6.16 μ_B. From Fig. 5a the observed value of the total moment is seen to be 3.83 μ_B at 350 K suggesting a remarkably strong short range, two-dimensional antiferromagnetic exchange at high temperatures. The value of μ_T steadily decreases with decreasing temperature and is 0.40 μ_B at 2.21 K. Although χ_M rises at very low temperatures, Fig. 5b, probably due to trace paramagnetic impurities, the dominant exchange is antiferromagnetic. The value of the Curie–Weiss constant, −117.2, obtained from a least-squares fit of the straight line portion of $1/\chi$ vs T, Fig. 5c, reinforces the antiferromagnetic behavior of Y_2Sr $FeCuO_{6.5}$. The magnetic behavior is very reminiscent of that of the 2-D antiferromagnet FeOCl, except that the 3-D exchange is much stronger in the present case as evidenced by the respective Neél temperatures of about 265 K vs 85 K for FeOCl (20). The very broad Neél maxima observed for these systems are in fact a hallmark of the two-dimensionality of the magnetic interactions

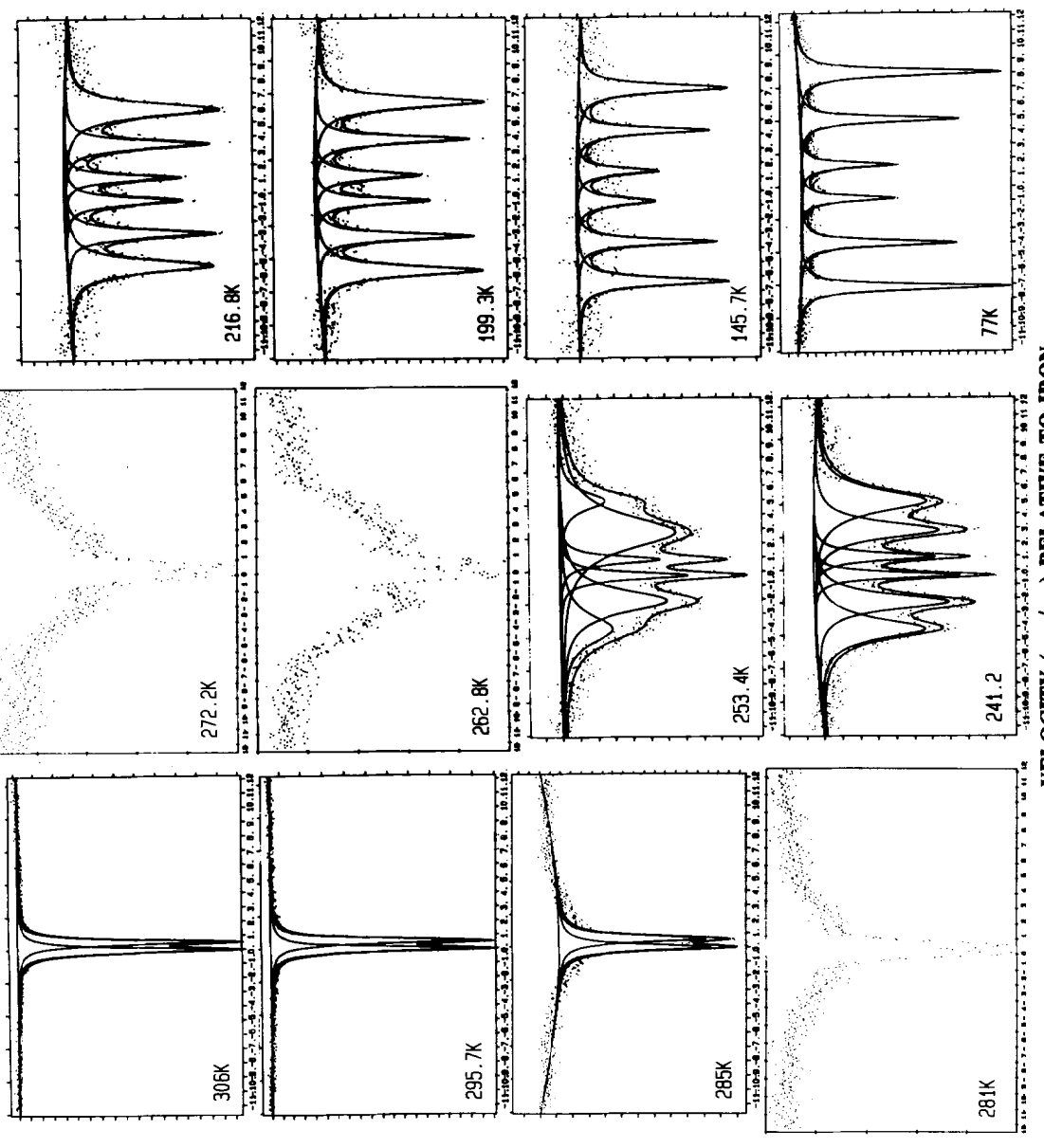

FIG. 3. Mössbauer spectra showing the transition from the rapidly relaxing paramagnetic to the three-dimensionally ordered magnetic state.

TABLE V

ISOMER SHIFTS, δ^a, QUADRUPOLE SPLITTINGS, ΔE; AND INTERNAL FIELDS, H_{int} FOR $Y_2SrFeCuO_{6.5}$

Temperature (K)	ΔE (mm/sec)	δ	H_{int} (kG)
306	0.56	0.26	0
295.7	0.57	0.25	0
295	0.54	0.25	0
285	0.61	0.28	>0
253.4			252
241.2			270
216.8			333
199.3			362
181.7			385
181.1			382
145.7			418
120.7			440
77			467
4.8			499

[a] Relative to natural iron metal foil.

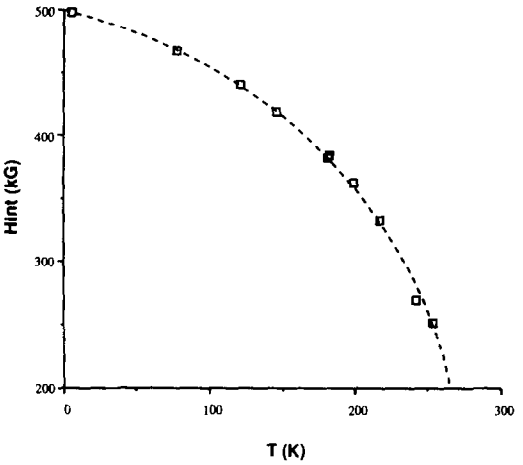

FIG. 4. Internal magnetic field vs temperature for $Y_2SrFeCuO_{6.5}$.

and fully consistent with the structurally induced anisotropy of the magnetic exchange.

Summary

The structure of $Y_2SrFeCuO_{6.5}$ can be considered a derivative of $Sr_3Ti_2O_7$ (4) in which double layers of one-apex sharing octahedra are separated by Y^{3+}. Numerous structures have been derived from this parent compound by the replacement of Ti^{4+} by lower valent transition metals and charge compensation by higher valent ions on the alkaline earth site. Thus the series of compounds $Ln_2AM_2O_7$, Ln^{3+} = La, Nd, Sm, Eu, Gd, Tb; A^{2+} = Sr, Ba; M^{3+} = Mn, Fe has been synthesized (*10, 21*). The replacement of Ti^{4+} with Cu^{2+} to form $La_2SrCu_2O_6$ requires the removal of an oxygen ion for overall charge neutrality. The apical oxygen joining the two octahedra is missing, resulting in layers of copper pyramids whose bases face each other (*11*). The lowering of the valence of the octahedral ion from 4+ to 3+ is charge compensated by trivalent rare earth ions and maintains the octahedral double layer. The replacement of the 4+ ion with Cu^{2+} introduces a modification in the structure by the removal of the apical O^{2-} to create separate copper pyramids. The replacement of $2Ti^{4+}$ in the parent compound by $Fe^{3+}Cu^{2+}$ again causes the removal of an oxygen ion, but now the unshared apex of the octahedron is lost. The structure of $YBaFeCuO_5$ contains double layers of apex-sharing Fe/Cu pyramids separated by a single layer of Y in 8-fold coordination—a fluorite unit (*14*). In $Y_2SrFeCuO_{6.5}$ the structure consists also of the apex-sharing Fe/Cu pyramids but they are separated by a double layer of defect fluorite units consisting of Y in 7-fold coordination. The centers of the pyramids are randomly occupied by Fe^{3+} and Cu^{2+}. An interesting metric relationship exists among these structures as shown in Table VI that emphasizes their common perovskite derived origin. Mössbauer spectra show a magnetic phase transition near 265 K. The paramagnetic phase coexists over an extended temperature range with the magnetically ordered phase, characteristic behavior for magnetic ordering in layer structures. The quadrupole splitting, isomer shift, and internal magnetic field values are

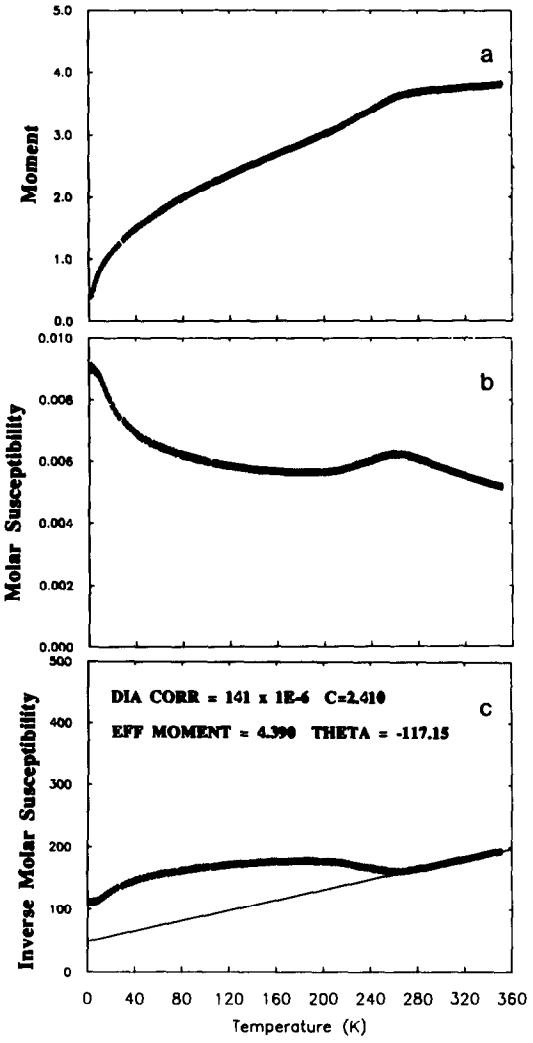

FIG. 5. Magnetic susceptibility parameters vs temperature for $Y_2SrFeCuO_{6.5}$.

consistent with high spin Fe^{3+} in 5-fold coordination. The spectra are from a single crystallographically distinct iron in agreement with the X-ray and neutron diffraction results. The Fe/Cu ratio does not deviate from 1 : 1 and there is no variable oxygen content. Of the rare earth elements only Gd and Er form this compound. This phase is structurally related to the Ruddlesden-Popper phase $Sr_{n+1}Ti_nO_{3n+1}$ with $n = 2$.

TABLE VI

LATTICE PARAMETERS AND SPACE GROUPS OF PHASES DERIVED FROM THE $Sr_3Ti_2O_7$ STRUCTURE. THE RELATIONSHIP TO THE PEROVSKITE LATTICE CONSTANT a_p IS INDICATED

Compound	a (Å)	b (Å)	c (Å)	Space group
$Sr_3Ti_2O_7$	3.90 a_p		20.38	*I*4 *mmm*
$La_2BaFe_2O_7$	3.933 a_p		20.85	*I*4/*mmm*
$Tb_2SrFe_2O_7$	5.506 $\sqrt{2}\,a_p$		19.65	$P4_2/mnm$
$La_2SrCu_2O_6$	3.86 a_p		19.88	*I*4/*mmm*
$NdSr_2Cu_2O_{5.76}$	3.7701 a_p	11.4381 $3a_p$	20.0938	*Immm* (22)
$YBaFeCuO_5$	3.867 a_p		7.656 $2a_p$	*P*4*mm*
$Y_2SrFeCuO_{6.5}$	5.4036 $\sqrt{2}\,a_p$	10.702 $2\sqrt{2}\,a_p$	20.250	*Ibam*

Acknowledgments

The first four authors acknowledge the support of the Robert A. Welch Foundation of Houston, Texas, and the Microelectronics and Computer Technology Corporation (MCC) of Austin, Texas. The research by P.L., S.P., and J.D.J. is supported by the US Department of Energy, Basic Energy Sciences/Materials Sciences under Contract W-31-109-ENG-38 and by NSF Science and Technology Center for Superconductivity Grant DMR88-09854. The authors thank Dr. Joel S. Miller and Mr. Scott McClean of the Central Research and Development Laboratory, DuPont Co., Wilmington, DE for the magnetic susceptibility measurements. W.M.R. also thanks the Northeastern University Research and Scholarship Development and Biomedical Support Funds for support to purchase a cobalt-57 Mössbauer spectroscopy source.

References

1. B. AURIVILLIUS, *Ark. Kemia.* **1,** 463 (1949).
2. B. AURIVILLIUS, ibid, **1,** 499 (1949).
3. B. AURIVILLIUS, ibid, **2,** 519 (1950).
4. S. N. RUDDLESDEN AND P. POPPER, *Acta Crystallogr.* **11,** 54 (1958).
5. J. G. BEDNORZ AND K. MÜLLER, *Z. Phys. B* **64,** 189 (1986).

6. S. A. SUNSHINE, L. F. SCHNEEMEYER, T. SIEGRIST, D. C. DOUGLASS, J. V. WASZCZAK, R. J. CAVA, E. M. GYORGY, AND D. W. MURPHY, *Chem. Mater.* **1,** 331 (1989).
7. D. J. WEHE, W. R. BUSING, AND H. A. LEVY, Program ORABS, ORNL, TM 229, Oak Ridge, TN (1962).
8. S. M. SHELDRICK, SHELX 76, Program for Crystal Structure Determination, University of Cambridge, England (1976).
9. "International Tables for X-Ray Crystallography" Vol. IV, Kynoch Press, Birmingham (1974). (Present distributor Kluwer Academic Publishers, Dordrecht).
10. D. SAMARAS, A. COLLOMB, AND J. JOUBERT, *J. Solid State Chem.* **7,** 337 (1973).
11. N. NGUYEN, L. ER-RAKHO, C. MICHEL, J. CHOISNET, AND B. RAVEAU, *Mater. Res. Bull.* **15,** 891 (1980).
12. J. D. JORGENSEN, J. FABER, JR., J. M. CARPENTER, R. K. CRAWFORD, J. R. HAUMANN, R. L. HITTERMAN, R. KLEB, G. E. OSTROWSKI, R. J. ROTELLA, AND T. G. WORLTON, *J. Appl. Crystallogr.* **22,** 321 (1989).
13. R. B. VON DREELE, J. D. JORGENSEN, AND C. G. WINDSOR, *J. Appl. Crystallogr.* **15,** 581 (1982).
14. L. ER-RAKHO, C. MICHEL, PH. LACORRE, AND B. RAVEAU, *J. Solid State Chem.* **73,** 531 (1988).
15. I. D. BROWN AND D. ALTERMATT, *Acta Crystallogr. Sect. B* **41,** 244 (1985).
16. J. B. GOODENOUGH, "Magnetism and the Chemical Bond" Interscience, New York, (1963).
17. P. D. BATTLE, T. C. GIBB, AND P. LIGHTFOOT, *J. Solid State Chem.* **84,** 237 (1990).
18. D. VAKNIN, S. K. SINHA, D. E. MONCTON, D. C. JOHNSTON, J. M. NEWSAM, C. R. SAFINYA, AND H. E. KING, JR., *Phys. Rev. Lett.* **58,** 2802 (1987).
19. D. P. E. DICKSON, F. J. BERRY, M. F. THOMAS, AND C. E. JOHNSON, "Mössbauer Spectroscopy," D. P. E. Dickson and F. J. Berry, Editors, Cambridge University Press, Cambridge, England, 1986.
20. S. M. KAUZLARICH, J. F. ELLENA, P. D. STUPIK, W. M. REIFF, AND B. A. AVERILL, *J. Amer. Chem. Soc.* **109,** 4561 (1987).
21. M. N. DESCHIZEAUX CHERUY AND J. C. JOUBERT, *J. Solid State Chem.* **40,** 14 (1981).
22. V. CAIGNAERT, R. RETOUX, C. MICHEL, M. HERVIEU, AND B. RAVEAU, *Physica C* **167,** 483 (1990).